Optics Letters

Second-harmonic-generation enhancement in cavity resonator integrated grating filters

François Renaud,[1,2,*] Antoine Monmayrant,[1] Stéphane Calvez,[1] Olivier Gauthier-Lafaye,[1] Anne-Laure Fehrembach,[2] and Evgeny Popov[2,3]

[1]*LAAS-CNRS, Université de Toulouse, CNRS, 7 avenue du colonel Roche, F-31400 Toulouse, France*
[2]*Aix Marseille Univ, CNRS, Centrale Marseille, Institut Fresnel, F-13013 Marseille, France*
[3]*Institut Universitaire de France, France*
*Corresponding author: francois.renaud@fresnel.fr

We demonstrate numerically and experimentally second-harmonic generation (SHG) in a cavity resonator integrated grating filter (CRIGF, a planar cavity resonator made of Bragg grating reflectors) around 1550 nm. SHG is modeled numerically for several different systems, including a thin plane layer of LiNbO$_3$ without and with a grating coupler to excite a waveguide mode. We demonstrate that when the waveguide mode is confined to a CRIGF, designed to work with focused incident beams, the SHG power is increased more than 30 times, compared to the case of a single grating coupler used with an almost collimated pump beam. © 2019 Optical Society of America

https://doi.org/10.1364/OL.44.005198

Non-linear nanophotonics has experienced a major boom over the past 15 years due to advances in modeling, component manufacturing, and the continuous development of laser sources and non-linear materials. Applications range from lasers to quantum information, spectroscopy, and high-resolution microscopy, with potential for manipulating and manufacturing nano-objects. Two major areas of research are currently being explored to harness the low non-linear susceptibilities of materials.

On one hand, ribbon and slab waveguides, either flat or structured, provide solutions to achieve the necessary phase matching between the pump wave(s) and the generated signal, so that non-linear interaction takes place constructively throughout the propagation distance of the guided modes [1–8]. The phase matching is achieved either by mode dispersion relation engineering or through grating assistance [1,2]. However, the necessary propagation length limits the compactness of the circuits, and the need for phase matching limits their versatility.

On the other hand, resonators, nanoparticles, and photonic crystal cavities exploit modes with long lifetimes to increase the duration of non-linear interaction [7,9–13]. But their low modal volumes limit the volume of non-linear interactions and make non-linear conversions very sensitive to manufacturing defects. Cavity resonator integrated grating filters (CRIGFs) are intermediate devices between waveguides and cavities

[14,15]. A CRIGF consists of a resonant grating of finite length functioning as a grating coupler (GC) integrated within a waveguide resonator, formed by two distributed Bragg reflectors (DBRs). When a focused beam illuminates the GC part of the CRIGF, a fraction of its energy is coupled into one mode of the structure, similar to what happens in a resonant waveguide grating (RWG). Since the mode field envelope is exponentially decreasing inside the DBRs, the electromagnetic energy is localized in the waveguide layer, under the GC. Contrary to the RWGs, the resonance wavelength of the CRIGF is determined mainly by the modes localized between the DBRs [16]. The GC can be considered as a perturbative outcoupler for these modes and thus must be designed so that its resonant wavelength is close to the cavity mode resonance [17].

In this Letter, we report on second-harmonic generation (SHG) enhancement in such structures, both theoretically and experimentally. We show that SHG is enhanced as compared to bulk material and to infinite gratings, without any requirement of phase matching for the SHG signal.

Figure 1 shows the CRIGF structure under study. It is based on a lithium-niobate-on-insulator (LNOI) substrate, which is a promising platform for non-linear optics [5,8], capitalizing on LiNbO$_3$'s strong non-linear susceptibility ($\chi^{(2)} = 33 \text{ pm} \cdot \text{V}^{-1}$) [18], the guided wave's low loss propagation, and high confinement provided by a thick insulator SiO$_2$ buffer. Here, the SiO$_2$ buffer is 2 µm thick, and the 300-nm-thick guiding layer and

Fig. 1. Schematic presentation of the CRIGF structure: dark gray, LiNbO$_3$, light gray SiO$_2$, orange Si$_3$N$_4$. The LiNbO$_3$ axes and layer thicknesses are indicated in the figure.

500-µm-thick substrate are made of x-cut crystalline LiNbO₃. The GC and the two DBRs are etched in a 72-nm-thick Si₃N₄ layer, and the structure is then encapsulated in a 323-nm-thick SiO₂ layer serving as an antireflection coating at 1.55 µm. The nominal filling factor (ratio between the groove width and the grating period) of GC is 0.55, and that of the DBRs is 0.5. The structure is considered infinite along the z direction. The vertical structure is designed to support only the fundamental TE₀ guided mode at the wavelength of 1.55 µm. To excite this guided mode, the first diffraction order of the GC is used. The period of the GC is determined by the grating equation at normal incidence, $\Lambda_{GC} = 10000 \frac{\lambda}{n_{eff}}$, with λ the fundamental wavelength and n_{eff} the effective index of the TE₀ mode. We use $\Lambda_{GC} = 865$ nm to center the resonance peak close to 1.555 µm. The period of the DBRs is chosen to couple the two counterpropagative modes in the structure. It can be shown that this period must be half of the GC period. The position of the resonance wavelength depends on the length of the cavity [15,19]. The length of the phase section (PS) (unetched Si₃N₄) between the DBR and the GC is numerically optimized to $L_{PS} = 627$ nm, so that the resonance wavelength falls in the middle of the DBR bandgap.

Numerically, to have an efficient reflection of the mode, 200-period-long DBRs are used. The number of GC periods is 21, which optimizes the CRIGF reflectivity for a focused incident beam with a radius at waist $w = 9$ µm. The refractive indices of the different layers at the fundamental frequency (1.55 µm)/SHG frequency (0.775 µm) are $n_{LiNbO_3} = 2.138/2.179$ (for the extraordinary index [20]), $n_{SiO_2} = 1.444/1.454$ [21], and $n_{Si_3N_4} = 1.996/2.026$ [22].

The CRIGF is studied numerically using the Fourier modal method (FMM) [17], adapted to calculate the SHG signal under the undepleted pump assumption according to [23]. The calculations are performed using 1401 Fourier components at the fundamental frequency, and 2801 at the second-harmonic frequency. The theoretical reflectivity and transmissivity spectra of the structure are plotted on Fig. 2 (dotted lines), together with SHG intensity. Note that the SHG intensity includes all diffraction orders and directions (in substrate and superstrate). Outside the resonance, the reflectivity of the structure is low, and the SHG signal is almost zero. At the resonance, one can observe a typical Fano-type anomaly, with the reflectivity rising sharply when the waveguide mode of the structure is excited [24], close to 1555 nm. The excitation of the mode leads to a sharp increase in the electromagnetic field inside the guiding nonlinear layer,
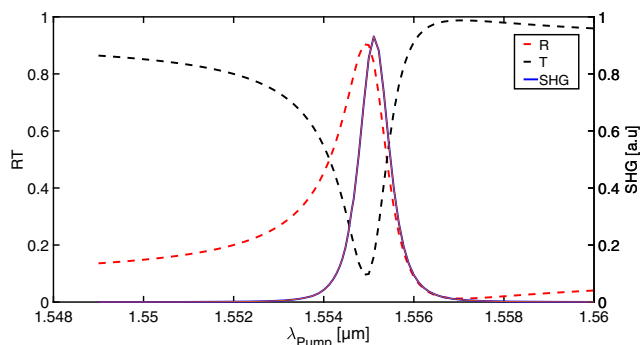
which results in a peak of the SHG power emitted by the structure. The SHG peak is slightly shifted from the reflectivity peak, because it is positioned at the maximum of the amplitude of the excited resonant mode (the pole of the scattered matrix [25,26]).

In order to evaluate the benefits of CRIGF for nonlinear optics, we compare it to four structures. The first one is the thin niobate film without any grating. The second one is made of the planar heterostructure with its SiO₂ buffer and the thick (about 500 µm) LiNbO₃ substrate. The third and fourth structures are the equivalent of the first one, adding the RWG (i.e., an infinitely long grating with the same parameters as the GC of the CRIGF), illuminated by either a large (100 µm radius at waist) or focused (9 µm radius at waist) beam. In all cases, the beam is incident along the x axis, with its electric field along the z axis, and the incident power is the same. In cases 1, 3–5, the beam has a Gaussian profile, and in case 2, we use a beam with a 9 µm half-width rectangular profile having the same power as in case 1. The thickness for the LiNbO₃ substrate (497 µm) is chosen to have a maximum of the non-phase-matched SHG generation. Hence, case 2 corresponds to an overestimated value of the maximum SHG that can be achieved in a bulk substrate with this orientation.

We stress that except for structure 2, the calculations are made without taking into account the SHG by the LiNbO₃ substrate. Our computational results are summarized in Table 1, and show that the CRIGF structure allows a much higher second-harmonic conversion than in the case of the classical resonant grating.

Our understanding of these results is the following. Without the grating coupler (structure 1), the waveguide mode cannot be excited, and the nonlinear layer is quite thin, so that the SHG signal is the weakest one, serving as a base for comparison. If we take into account the SHG in the ~500 µm-thick substrate (structure 2), the signal is increased almost 800 times.

By adding a grating to the first structure (lines 3 and 4 of the Table), the SHG signal is much stronger than in case 1. Calculation for an infinite corrugated waveguide shows that the mode effective index is equal to $1.7955 + i1.617 \times 10^{-3}$. It is easy to demonstrate that the small imaginary part of the effective index requires incident a beam radius at the waist on the order of 150 µm (i.e., $\lambda/(2\pi \times 1.617 \times 10^{-3})$; see [25]) for an efficient excitation of the mode. When the structure is illuminated by a large, almost collimated beam, which properly excites the guided mode (i.e., its beam divergence lies within the angular acceptance of the RWG), the SHG is two times stronger than that of the substrate (1600 times thicker) and 1500 times stronger than that of the unstructured plane (reference case 1). Going to a smaller beam waist in order to enhance the fundamental beam power density does not enhance the

Fig. 2. Theoretical reflection, transmission, and SHG power versus the pump wavelength.

Table 1. Numerical Comparison of SHG Powers Emitted by Different Structures

Ref.	Structure	Radius at Waist [µm]	SHG [arb. u.]	Guided Mode Amplitude [arb. u.]
1	Single niobate layer	9	1	N.A.
2	+497 µm	9	731	N.A.
3	RWG	100	1500	7.212
4	RWG	9	32	2.289
5	CRIGF	9	51667	12.74

SHG for RWGs. Indeed, when used with a tightly focused beam of 9 µm waist, the RWG efficiency is strongly decreased because the beam divergence strongly exceeds the RWG angular acceptance [24,27]. We see in Table 1 that the guided mode amplitude is three times smaller than with a large beam, despite the 11-fold increase in power density induced by the stronger focusing. As a result, the SHG power emission from this structure lies in between the performances of the non-structured thin and thick layers (cases 1 and 2).

On the contrary, CRIGFs were designed to handle focused beams. It can be seen in Table 1 that the guided mode amplitude almost doubles between structures 3 and 5, which leads to an SHG output increase by a factor greater than 30. One can also see that the ratio of the guided modes squared intensities (i.e., the fourth power of the mode amplitudes) between structures 3 and 4 is on the same order of magnitude as the ratio of the SHG efficiency for these two structures. It is another indication that the efficiency of CRIGF for SHG arises from the efficient coupling of the pump beam to the localized guided mode.

To conclude this numerical study, we computed the ratio $\eta = P_{2\omega}/[P_\omega]^2$ with $P_{2\omega}$ the total SHG power extracted from the device and P_ω the fundamental incident power. For the CRIGF (line 5, table 1), $\eta = 8.2 \times 10^{-6}$ W^{-1} (giving a conversion efficiency of 3.2 W$^{-1} \cdot$ cm^{-2} over the area of the 9-µm-waist Gaussian beam). 82% of this power is coupled out into the reflected zeroth order of the GC (6.7×10^{-6} W^{-1}) and 15% (1.2×10^{-6} W^{-1}) into the transmitted zeroth order. We thus predict conversion efficiency for this CRIGF at least 50× greater than what is reported in the literature for RWG [1,28] and 10× smaller than for waveguides [29].

The experimental demonstration is based on a LNOI substrate from NanoLN. The fabricated structure is as described above (see Fig. 1) with a finite transverse size of 50 µm along z. The Si$_3$N$_4$ is deposited by inductively coupled plasma – plasma enhanced chemical vapor deposition (ICP-PECVD) at a low temperature (100°C). The CRIGF is then patterned by soft-mold nano-imprint lithography [30] and etched in the Si$_3$N$_4$ layer by reactive ion etching (RIE). The topmost LiNbO$_3$ layer acts as a stop-etch, resulting in a smooth and homogenous grating, as confirmed by atomic force microscope (AFM) measurements. The final SiO$_2$ layer is deposited by ICP-PECVD.

The characterization setup is shown in Fig. 3. A fibered CW tunable laser (Santec TSL-550) amplified by an erbium-doped fiber amplifier (EDFA) is used, outputting up to 25 mW in the 1.55 µm range. The beam is then collimated and focused to achieve a waist of 9 µm (half the size of the GC part) on the CRIGF. The reflected and transmitted signals, at the fundamental frequency, are measured by two InGaAs photodiodes (Thorlabs PDA20CS-EC). The SHG generated by the CRIGF is collimated using a $f = 18$ mm, NA = 0.2 lens, separated from the fundamental signal using a dichroic beam splitter and then focused into a multimode fiber (400 µm core, NA = 0.39) using a parabolic mirror, and measured using a spectrometer (Flame Ocean Optics, 1.5 nm resolution).
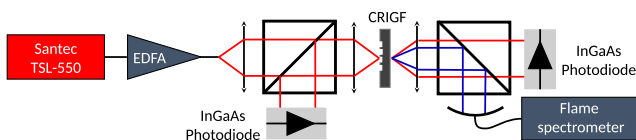
In this configuration, only the transmitted zeroth diffraction order of the GC is collected. The SHG power reflected and the SHG power in the ±1st diffraction orders of the GC are not collected.

Figure 4 shows the SHG intensity measured versus the pump wavelength and the second-harmonic wavelength. It should be noted that the SHG spectrum is enlarged by the instrument response of our spectrometer. The wavelength of the SHG evolves with the pump wavelength. A linear regression on the experimental SHG maximum emission wavelength (gray dots in Fig. 4) versus pump wavelength yields a slope of 1/2, with a precision limited by the resolution and the noise of our spectrometer.

When the pump wavelength lies outside the CRIGF resonance (between 1554 nm and 1555.5 nm), a weak SHG power is measured, which corresponds to the power emitted by the LiNbO$_3$ substrate. Close to the resonance wavelength of the CRIGF (1555 nm), the SHG power increases sharply. As discussed above, this is due to the excitation of the guided mode at the fundamental frequency, which increases the electric field inside the LiNbO$_3$ layer. The SHG power emitted when the pump beam is focused on the CRIGF is at least 60 times higher than the power emitted when the pump is focused on a non-structured part of the sample. This is comparable to the 70-times underestimated difference between the numerical results given in Table 1 (lines 2 and 5). It must also be taken into account that the experimental results contain only measurements of the zeroth transmitted diffraction order of the GC at the second-harmonic frequency. The power measured in the zero transmitted order is 0.6 nW for a 17.7 mW incident beam, leading to an experimental η ratio in the zero transmitted order of 1.9×10^{-6} W^{-1}, comparable to the theoretical value (1.2×10^{-6} W^{-1}).

The SHG emission occurs only for TE-polarized fundamental light, confirming that it results from light coupled into the CRIGF to a TE mode, and the SHG signal is also TE polarized, co-linear with the pump polarization, which corresponds to a type I conversion, as expected from calculations.

Figure 5 shows the evolution of the SHG power as a function of the pump power on a log-log scale. Its analysis shows that, as expected within the assumption of an undepleted pump, the SHG power depends quadratically on the fundamental power.

In addition, two other CRIGFs were fabricated and investigated, having different periods of the GC (845 nm and 885 nm, with DBR periods and PS lengths modified accordingly). They are characterized by fundamental resonances at

Fig. 3. Schematic of the experimental characterization setup.
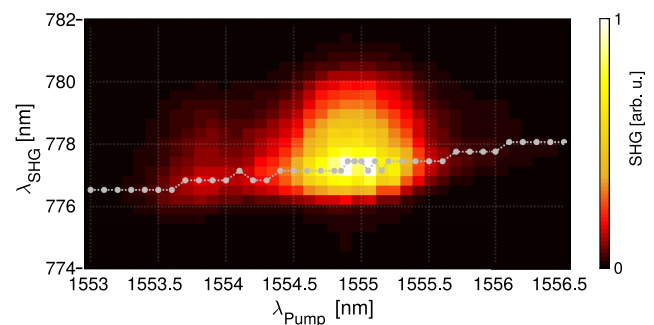
Fig. 4. SHG intensity as a function of both pump and SHG wavelengths (gray dots correspond to the maximum of SHG for each pump wavelength). Pump power, 25 mW.
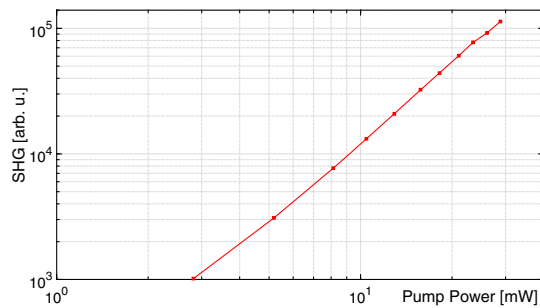
Fig. 5. SHG power as a function of the pump power.
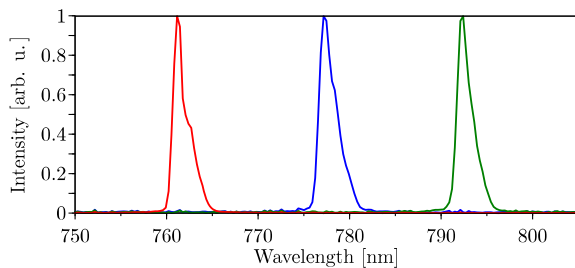
Fig. 6. Normalized SHG spectrum for three CRIGFs with GC periodicity of 845 nm (red), 865 nm (blue), and 885 nm (green).

1525 nm and 1585 nm, respectively. The SHG spectra of the three different devices are presented in Fig. 6.

Resonant SHG emission was also observed with the latter two structures, with the expected 0.5 linear dependence of the SHG wavelength with respect to the excitation resonance wavelength. This shows the intrinsic versatility of this design, where a simple adjustment of the period allows to chose the resonant wavelength on the same vertical structure, without taking into account any phase-matching consideration.

We demonstrated successful SHG enhancement in CRIGF structures made upon LNOI at 1.55 µm. The comparison with the SHG signal obtained with the non-structured LNOI and the LNOI structured with a RWG demonstrates the interest in CRIGF for SHG enhancement. The gain is due mainly to the fact that as compared to the RWG, the CRIGF allows a stronger excitation of the mode with a focused beam. Moreover, simply changing the period of the grating on the same vertical stack and tuning the excitation wavelength leads to SHG over the whole C-band. The theoretical and experimental results are in good agreement, validating our modeling of SHG in CRIGF with the FMM. This first result paves the way to more efficient designs, exhibiting, for example, resonant enhancement at both pump and SHG wavelengths and designed for phase matching. Due to our first calculations of such designed CRIGF, we can expect conversions with more than one order of magnitude greater efficiency.

REFERENCES

1. G. Blau, E. Popov, F. Kajzar, A. Raimond, J. Roux, and J. Coutaz, Opt. Lett. **20**, 1101 (1995).
2. A. Cowan and J. Young, Phys. Rev. B **65**, 085106 (2002).
3. M. Siltanen, S. Leivo, P. Voima, M. Kauranen, P. Karvinen, P. Vahimaa, and M. Kuittinen, Appl. Phys. Lett. **91**, 111109 (2007).
4. G. Poberaj, H. Hu, W. Sohler, and P. Günter, Laser Photon. Rev. **6**, 488 (2012).
5. C. Wang, K. Zhaoyi, L. Myoung-Hwan, X. Xiong, X.-F. Ren, G.-C. Guo, N. Yu, and M. Loncar, Nat. Commun. **8**, 2098 (2017).
6. C. Wang, X. Xiong, N. Andrade, V. Venkataraman, X.-F. Ren, G.-C. Guo, and M. Loncar, Opt. Express **25**, 6963 (2017).
7. M. Borghi, C. Castellan, S. Signorini, A. Trenti, and L. Pavesi, J. Opt. **19**, 093002 (2017).
8. A. Boes, B. Corcoran, L. Chang, J. Bowers, and A. Mitchell, Laser Photon Rev. **12**, 1700256 (2018).
9. J. Bravo-Abad, S. Fan, S. Johnson, J. Joannopoulos, and M. Soljacic, J. Lightwave Technol. **25**, 2539 (2007).
10. N. Segal, S. Keren-Zur, N. Hendler, and T. Ellenbogen, Nat. Photonics **9**, 180 (2015).
11. A. D. Logan, M. Gould, E. R. Shmidgall, K. Hestroffer, Z. Lin, W. Jin, A. Majumdar, F. Hatami, A. W. Rodriguez, and K.-M. C. Fu, Opt. Express **26**, 33687 (2018).
12. A. Krasnok, M. Tymchenko, and A. Alù, Mater. Today **21**(1), 8 (2018).
13. R. Mohsen, G. Leo, I. Brener, A. V. Zayats, S. A. Maier, C. De Angelis, and H. E. A. Tan, Opto-Electronic Adv. **1**, 18002101 (2018).
14. K. Kintaka, T. Majima, J. Inoue, K. Hatanaka, J. Nishii, and S. Ura, Opt. Express **20**, 1444 (2012).
15. X. Buet, E. Daran, D. Belharet, F. Lozes-Dupuy, A. Monmayrant, and O. Gauthier-Lafaye, Opt. Express **20**, 9322 (2012).
16. R. Laberdesque, O. Gauthier-Lafaye, H. Camon, A. Monmayrant, M. Petit, O. Demichel, and B. Cluzel, J. Opt. Soc. Am. A **32**, 1973 (2015).
17. N. Rassem, E. Popov, and A.-L. Fehrembach, Opt. Quantum Electron. **47**, 3171 (2015).
18. M. J. Weber, *Handbook of Optical Materials* (CRC press, 2018).
19. S. Ura, J. Inoue, K. Kintaka, and Y. Awatsuji, in *13th International Conference on Transparent Optical Networks* (2011), pp. 1–4.
20. D. Nelson and R. Mikulyak, J. Appl. Phys. **45**, 3688 (1974).
21. I. H. Malitson, J. Opt. Soc. Am. **55**, 1205 (1965).
22. K. Luke, Y. Okawachi, M. R. E. Lamont, A. L. Gaeta, and M. Lipson, Opt. Lett. **40**, 4823 (2015).
23. W. Nakagawa, R.-C. Tyan, and Y. Fainman, J. Opt. Soc. Am. A **19**, 1919 (2002).
24. E. Popov, L. Mashev, and D. Maystre, Opt. Acta **33**, 607 (1986).
25. M. Nevière, *Electromagnetic Theory of Gratings*, R. Petit, ed. (Springer-Verlag, 1980), p. 152.
26. M. Nevière, E. Popov, R. Reinisch, and G. Vitrant, *Electromagnetic Resonances in Nonlinear Optics* (Gordon and Breach, 2000), chap. 6 and 10.
27. S. S. Wang and R. Magnusson, Appl. Opt. **32**, 2606 (1993).
28. T. Ning, H. Pietarinen, O. Hyvärinen, R. Kumar, T. Kaplas, M. Kauranen, and G. Genty, Opt. Lett. **37**, 4269 (2012).
29. C. Wang, C. Langrock, A. Marandi, M. Jankowski, M. Zhang, B. Desiatov, M. M. Fejer, and M. Loncar, Optica **5**, 1438 (2018).
30. S. Pelloquin, S. Augé, K. Sharshavina, J.-B. Doucet, A. Héliot, H. Camon, A. Monmayrant, and O. Gauthier-Lafaye, in *Symposium on Design, Test, Integration and Packaging of MEMS/MOEMS (DTIP)* (2018).